

# Ambient Backscatterers Using FM Broadcasting for Low Cost and Low Power Wireless Applications

Spyridon Nektarios Daskalakis<sup>1</sup>, *Student Member, IEEE*, John Kimionis<sup>2</sup>, *Student Member, IEEE*,  
Ana Collado, *Senior Member, IEEE*, George Goussetis, *Senior Member, IEEE*,

Manos M. Tentzeris, *Fellow, IEEE*, and Apostolos Georgiadis<sup>3</sup>, *Senior Member, IEEE*

**Abstract**—Nowadays, the explosive growth of Internet-of-Things-related applications has required the design of low-cost and low-power wireless sensors. Although backscatter radio communication is a mature technology used in radio frequency (RF) identification applications, ambient backscattering is a novel approach taking advantage of ambient signals to simplify wireless system topologies to just a sensor node and a receiver (RX) circuit eliminating the need for a dedicated carrier source. This paper introduces a novel wireless tag and RX system that utilizes broadcast frequency modulated (FM) signals for backscatter communication. The proposed proof-of-concept tag comprises of an ultralow-power microcontroller (MCU) and a RF front-end for wireless communication. The MCU can accumulate data from multiple sensors through an analog-to-digital converter, while it transmits the information back to the RX through the front-end by means of backscattering. The front-end uses ON-OFF keying modulation and FM0 encoding on ambient FM station signals. The RX consists of a commercial low-cost software-defined radio which downconverts the received signal to baseband and decodes it using a suitable signal processing algorithm. A theoretical analysis of the error rate performance of the system is provided and compared to bit-error-rate measurements on a fixed transmitter-tag-RX laboratory setup with good agreement. The prototype tag was also tested in a real-time indoor laboratory deployment. Operation over a 5-m tag-reader distance was demonstrated by backscattering information at 2.5 kb/s featuring an energy per packet of 36.9  $\mu$ J.

**Index Terms**—Ambient backscattering, backscatter communication, frequency modulated (FM) modulation, inkjet printing, Internet-of-Things (IoT), radio frequency (RF) identification (RFID) sensors, software-defined radio (SDR).

Manuscript received June 30, 2017; revised September 16, 2017; accepted October 12, 2017. Date of publication November 9, 2017; date of current version December 12, 2017. This work was supported by the EU COST Action IC1301 WiPE. The work of S. N. Daskalakis was supported by the Lloyds Register Foundation (LRF) and the International Consortium in Nanotechnology (ICON). The work of A. Collado and A. Georgiadis was supported in part by the EU H2020 Marie Skłodowska-Curie under Grant 661621 and in part by COST Action IC1301 Wireless Power Transmission for Sustainable Electronics. The work of J. Kimionis and M. M. Tentzeris was supported in part by the National Science Foundation and in part by the Defense Threat Reduction Agency. This paper is an expanded version from the 2017 IEEE MTT-S International Microwave Symposium Conference, Honolulu, HI, USA, June 4–9, 2017. (*Corresponding author: Spyridon Nektarios Daskalakis.*)

S. N. Daskalakis, A. Collado, G. Goussetis, and A. Georgiadis are with the School of Engineering and Physical Sciences, Institute of Sensors, Signals, and Systems, Heriot-Watt University, EH14 4AS Edinburgh, U.K. (e-mail: sd70@hw.ac.uk; a.collado\_garrido@hw.ac.uk; g.goussetis@hw.ac.uk; apostolos.georgiadis@ieee.org).

J. Kimionis and M. M. Tentzeris are with the School of Electrical and Computer Engineering, Georgia Institute of Technology, Atlanta, GA 30332-250 USA (e-mail: ikimionis@gatech.edu; etentze@ece.gatech.edu).

Color versions of one or more of the figures in this paper are available online at <http://ieeexplore.ieee.org>.

Digital Object Identifier 10.1109/TMTT.2017.2765635

## I. INTRODUCTION

RECENTLY, Internet-of-Things (IoT) has become the trend for networking every day objects so as to automate and make easier our daily lives. The most important challenge for IoT applications, is the minimization of the cost and energy dissipation of the sensors. Keeping the massive number of energy-constrained IoT sensors active with low cost designs is a key issue. Commercial radio modules used in IoT devices typically use power-hungry radio frequency (RF) chains including oscillators, mixers and digital-to-analog converters (DACs) resulting in significant limitations of the battery life. One particularly promising approach to alleviate these issues is backscatter communication [1] that allows IoT sensor nodes-tags to transmit data by reflecting and modulating an incident RF wave [2]. Communication using backscatter principles has been widely deployed in the application of RF identification (RFID) for passive tags. The RF front-end part of the tags consists of only one RF transistor or switch. In this case the tags are battery-free and can operate using only RF power transmitted from an RFID reader resulting in communication ranges up to several meters [3], [4].

Ambient backscattering is an idea based on the bistatic backscatter philosophy and could constitute a very promising novel approach for extremely low power and low cost communication systems [5]. Utilizing ambient signals for backscattering, the communication scheme is simplified since it requires only a receiver (RX) eliminating the need for a continuous wave (CW) emitter. For example, ambient backscattering devices, such as RFID tags, can communicate with a reader by backscattering ambient RF signals that are available from multiple sources, such as mobile communications, television [5], frequency modulated (FM) radio [6], and WiFi [7] that are typically widely available in urban areas indoors and outdoors during day and night. In [5], two battery-free tags communicate via ambient backscatter TV signals. In [7], a WiFi backscatter deployment was designed to connect battery-free devices with off-the-shelf WiFi devices. Also a full-duplex ambient communication system was introduced in [8], where a WiFi access point can cooperate with backscatter IoT sensors with high data throughput. The use of ambient RF signals as the only source of both the CW carrier and the tag power is an extremely energy-efficient communication technique compared to the general backscattering technique.

In [9], preliminary results for a wireless sensor node prototype for agricultural monitoring were presented. The sensor

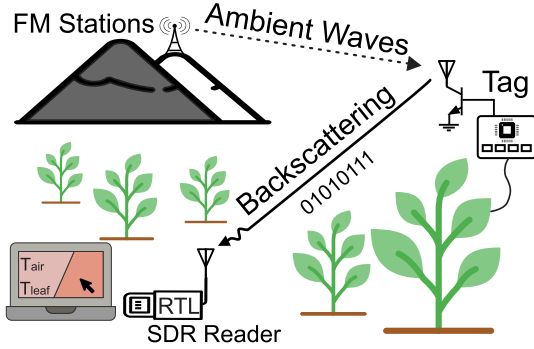


Fig. 1. Deployment of ambient backscattering in smart agriculture applications. Backscatter communication is achieved using ambient FM signals. The differential temperature ( $T_{\text{leaf}} - T_{\text{air}}$ ) is measured by the tag-sensor and is transmitted back to an SDR RX.

node measures the temperature difference between the leaf and the atmosphere in order to estimate the water stress of a plant [10]. The tag modulates and reflects a fraction of the ambient FM station signals back to the reader as it is shown in Fig. 1.

This paper is an extensive presentation of the novel ambient FM backscatter monitoring system [9] with low complexity and low power. We propose an improved version of this system for generic environmental monitoring applications by designing an improved RX algorithm. In addition to the RX implementation, we provide additional details about the tag circuitry, a theoretical tag-RX framework for the operation of the ambient backscatter system and a series of packet error rate (PER) and bit error rate (BER) measurements in a proof-of-concept indoor environment. The operation of the system prototype was demonstrated in the lab using an existing FM transmitter (TX) broadcasting 34 km away from the tag. Operation over a 5-m tag-to-reader distance was achieved by backscattering sensor data at 0.5, 1, and 2.5 kb/s bit rates.

Our work is different from [5], which first proposed ambient backscattering, in that it used ambient digitally modulated television signals whereas the system proposed in this paper uses analog FM signals. Also, a moderately expensive software defined USRP-N210 radio ( $\sim 1 - 5$  KUSD) used in [5] to receive and decode the signals whereas in our work a low cost Realtek (RTL) software-defined radio (SDR) (22 USD) was used. Recently, Wang *et al.* [6] also proposed ambient backscattering using FM signals but only for two state frequency-shift-keying modulated signals. In our work we used ON-OFF keying (OOK) modulation with FM0 encoding. In addition, an arbitrary waveform generator was used in [6] to generate the ambient FM signals contrary to signals from existing broadcast FM stations in this paper. Therefore, this paper takes into account all the signal characteristics of an FM radio broadcasting and serves as the proof-of-concept for practical ambient backscatter deployments. The findings reported are equally useful for indoors and outdoors, where FM broadcasting signals are pervasive.

The structure of this paper is as follows. Section II provides the principles of ambient backscatter communication. Section III describes the design and implementation of the sensor node-tag parts. Section IV provides the theory and

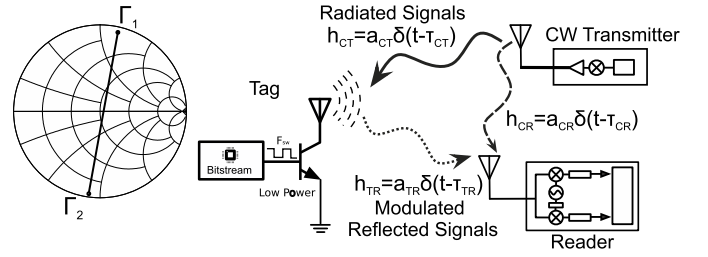


Fig. 2. Two-state antenna  $S_{11}$  parameters on a Smith chart (left). Bistatic backscatter principle (right). The emitter transmits a carrier signal and the tag reflects a small amount of the approaching signal back to the reader. The tag modulates the backscattered signal by changing the load connected to its antenna terminals resulting in a  $\Gamma_i$  change between two values (states).

performance analysis of the FM ambient backscatter system. Section V discusses the hardware and software part of the low cost RX. Section VI presents proof-of-concept experimental results, including an indoor demonstration and range measurements. Finally, Section VII includes concluding remarks.

## II. FM AMBIENT BACKSCATTERING

### A. Backscatter Principles

A general bistatic backscatter system consists of three devices: a backscatter node (i.e., a tag), a reader and a CW emitter. The tag receives a CW carrier signal with frequency  $F_c$  and scatters a fraction of it back to the reader as shown in Fig. 2 (right). It superimposes the sensor information on top of the carrier by appropriately changing the load connected to its antenna terminals according to [11]

$$\Gamma = \frac{Z_L - Z_a^*}{Z_L + Z_a} \quad (1)$$

with  $Z_L$  and  $Z_a$  denoting the load and the tag antenna impedance. For binary modulation, the reflected signal is modulated by switching the load between two discrete values ( $Z_1$  and  $Z_2$ ) effectively resulting in two reflection coefficient values, ( $\Gamma_1$  and  $\Gamma_2$ ) over time. The  $180^\circ$  difference between the two load values [Fig. 2 (left)] is necessary for maximization of backscatter performance. The reader captures the reflected signal at a frequency  $f_c + \Delta F$  and an additional phase  $\phi$  and then filters out the high frequency components.  $\Delta F$  is the carrier frequency offset (CFO) between the emitter and the reader. According to [12], the received signal can be expressed in the following complex baseband form:

$$y_r(t) = n(t) + \frac{A_c}{2} e^{-j2\pi \Delta F t} \times [a_{CR} e^{-j\phi_{CR}} + s a_{CT} a_{TR} e^{-j\phi_{CTR}} \Gamma(t - \tau_{TR})] \quad (2)$$

where  $A_c$  is the carrier amplitude,  $a_{CR}$ ,  $a_{CT}$ ,  $a_{TR} \in \mathbb{R}$  and  $\phi_{CR}$ ,  $\phi_{CTR} \in [0, 2\pi)$ . Moreover  $\tau_{TR}$  is the time delay constant of the tag-reader channel. Term  $s$  is related to the tag scattering efficiency and tag antenna gain at a given direction. The term  $a_{CR} e^{-j\phi_{CR}}$  defines the component which depends on the emitter-to-reader channel ( $h_{CR}$  in Fig. 2). The tag signal is a direct function of  $\Gamma$  over time and the term  $a_{CT} a_{TR} e^{j\phi_{CTR}}$  scales and rotates the modulated part of the tag signal. This term depends on the transmitter-to-tag and tag-to-reader channel parameters ( $h_{CT}$  and  $h_{TR}$  in Fig. 2). Finally,  $n(t)$  is the complex thermal Gaussian noise at the RX.

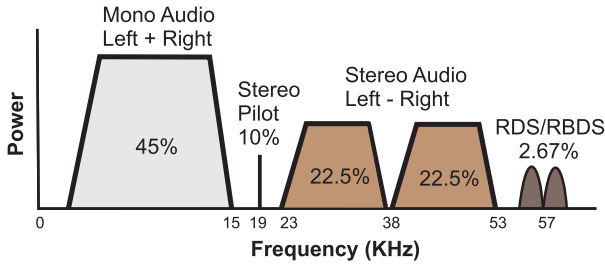


Fig. 3. Baseband Spectrum of a generic modern-day FM audio station. The signal contains left (L) and right (R) channel information (L + R) for monophonic and stereo reception.

### B. FM Broadcasting Operation

The FM broadcasting technology was first utilized in 1940 radio-audio transmissions and nowadays FM radio broadcasts take place between radio frequencies of 88 to 108 MHz with a channel bandwidth of 200 kHz. Each FM station uses frequency modulation in order to transmit the audio signals and the information signals varying the frequency of a carrier wave accordingly. A typical FM output signal is given by the following equation [13]:

$$x_{\text{FM}}(t) = A_c \cos \left[ 2\pi f_c t + 2\pi K_{\text{VCO}} \Delta f \int_0^t m(x) dx \right] \quad (3)$$

where  $m(x)$  is the baseband message signal, and  $\Delta f$  is the frequency deviation which is equal to the maximum frequency shift from  $f_c$  while  $K_{\text{VCO}}$  is the gain of the TX's voltage-controlled oscillator (VCO). Generally, it is not straightforward to analyze the properties of  $x_{\text{FM}}(t)$  due to its nonlinear dependence to the  $m(x)$ . The baseband message signal of a typical FM station as shown in Fig. 3 can be expressed as

$$m(t) = A_0[S_L(t) + S_R(t)] + A_1 \cos(2\pi f_1 t) + A_0 \times [S_L(t) - S_R(t)] \cos(2\pi f_2 t) + A_2 \text{RDS}(t) \cos(2\pi f_3 t) \quad (4)$$

with  $f_1 = 19$  kHz,  $f_2 = 38$  kHz, and  $f_3 = 57$  kHz. The  $S_L$  and  $S_R$  define the time domain signals from the “stereo left” and “stereo right” channels, respectively, while  $\text{RDS}(t)$  is the time domain signal of the Radio Data System (RDS) and Radio Broadcast Data System (RBDS). The gain factors  $A_0$ ,  $A_1$ , and  $A_2$  are used to appropriately scale the amplitude of  $S_L$  and  $S_R$  waveforms. As it can be easily observed in Fig. 3, the 0–15 kHz part of the message signal consists of the left and right channel information [(left) + (right)] for monophonic sound. Stereophonic sound is the result of the amplitude modulation of the [(left) – (right)] message onto a suppressed 38-kHz subcarrier in the 23–53-kHz region of spectrum. Furthermore, there is a 19-kHz pilot tone to enable RXs to recognize and decode the two stereo channels. Modern FM radio signals also include a 57-kHz subcarrier that carries RDS and RBDS data.

### C. Ambient FM Backscatter

In the case of typical ambient FM backscatter systems, incident “CW carrier” to the tag antenna is the signal in (3). The SDR RX receives the superposition of this signal and

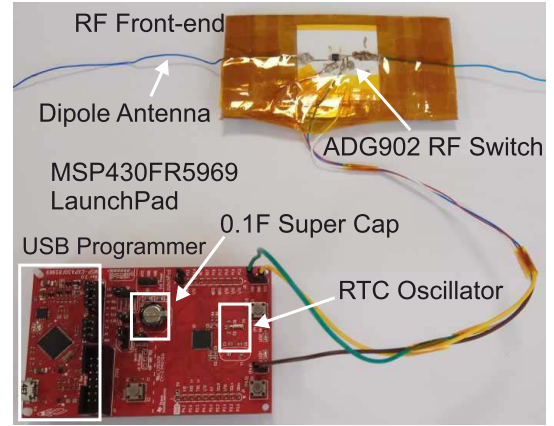


Fig. 4. Proposed tag prototype consists of an MSP430 development board [14] connected with an RF front-end board. The RF front-end consists of the ADG902 RF switch and was fabricated using inkjet printing technology on a paper substrate. An MCU digital output pin was connected with the control signal of the RF switch. The operation power of RF front-end was supplied by the MCU development board and the whole system was supplied by an embedded super capacitor for duty cycle operation.

the backscattered tag signal. Following the same procedure described in [12], but using an FM modulated carrier instead of a CW signal one may obtain the following complex baseband signal at the RX:

$$y_{\text{amb}}(t) = n(t) + \frac{A_c}{2} e^{-j2\pi \Delta F t} \times [\alpha_{\text{CR}} e^{-j\phi_{\text{CR}}} e^{-jM(t-\tau_{\text{CR}})} + s\alpha_{\text{CTR}}\alpha_{\text{TR}} e^{-j\phi_{\text{CTR}}} e^{-jM(t-\tau_{\text{TR}})} \Gamma(t-\tau_{\text{TR}})] \quad (5)$$

and

$$M(t) = 2\pi K_{\text{VCO}} \Delta f \int_0^t m(x) dx. \quad (6)$$

The received signal  $y_{\text{amb}}$  contains the desired information  $\Gamma$  but also the carrier, FM modulation and frequency offset. The magnitude square of the received complex waveform will be formulated below in order to eliminate the frequency offset. If the desired magnitude square is formed, a component proportional to the desired information will be generated along with dc and other interference terms. We show theoretically and experimentally in Sections IV and VI, respectively, that it is possible to successfully decode the signal provided there is a sufficiently high signal-to-noise-ratio (SNR).

## III. TAG DESIGN

### A. Tag

The main DIGITAL part of proposed tag is based on a 16-bit microcontroller (MCU) development board MSP-EXP430FR5969 [14] (Fig. 4). The development board is powered from a 0.1-F supercapacitor. The tag also includes a real-time clock (RTC) to wake up the MCU from the “sleep” operation mode, where the current consumption of the board is  $0.02 \mu\text{A}$ . The MCU generates 50% duty cycle pulses that control the RF switch, thus generating an OOK modulated backscattered signal. The OOK modulation is described in more detail in Section III-B. The MCU was programmed at 1-MHz clock speed using the internal local oscillator.

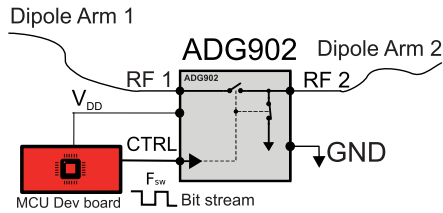


Fig. 5. Schematic of the RF switch utilized for the load modulation and of the dipole antenna arms.

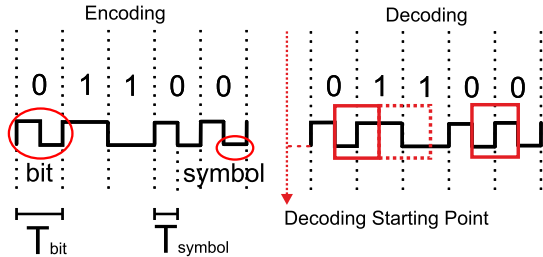


Fig. 6. In FM0 encoding, the boundaries of the bits must always be different. Two sequential “ON” or “OFF” correspond to the bit “1” (left). FM0 decoding technique, after shifting by  $T_{\text{symbol}}$ , RX has to detect only two possible pulse shapes (line square or dashed line square) (right).

The current consumption at 1 MHz was 126  $\mu\text{A}$  at 2.3 V (290  $\mu\text{W}$ ).

The MCU has a 16-channel 12-bit analog-to-digital converter (ADC) which was used to read analog output signals from sensors. In this paper, the tag is programmed to read four analog inputs and the voltage level of the super capacitor. These analog inputs can be used to provide information from out to four sensors. This paper focuses on the telecommunication aspect of the system and specific sensing examples form part of future work. When a tag wants to communicate with the reader, it sends a packet that contains the information of only one sensor each time. In [9], only two ADC inputs for two high precision, analog temperature sensors were used.

The backscatter communication of the tag is achieved with a separate RF front-end board. It consists of a 1.5-m wire dipole antenna in order to resonate within the FM band (95 MHz) and a single-pole, single-throw RF switch ADG902 by Analog Devices. The circuit schematic of the front-end is provided in Fig. 5, while the fabricated prototype is shown in Fig. 4.

The switch element varies the antenna load between two impedance values and is selected due to its low insertion loss ( $\sim 0.5$  dB @ 100 MHz) and high off isolation ( $\sim 57.5$  dB @ 100 MHz). The RF switch is a CMOS reflect-mode (i.e., not terminated) switch with high off-port VSWR and consumes less than 1  $\mu\text{A}$  at 2.75 V [15]. It is driven by a digital output of the MCU as shown in Fig. 5. The power consumption of the RF switch follows the equation  $(1/2)C_{\text{RF}}V_{\text{DD}}^2F_{\text{sw}}$ , which is the CMOS dynamic consumption [16]. The  $F_{\text{sw}}$  is the control switching frequency and  $C_{\text{RF}}$  the dynamic power dissipation capacitance at RF path when it is ON. For  $F_{\text{sw}} = 2.5$  kHz, which equals to our maximum bit rate 2.5 Kb/s,  $V_{\text{DD}} = 3.3$  V, and  $C_{\text{RF}} = 1.2$  pF (@ 1 MHz) the power consumption is estimated at 16.3 nA. As the data rate increases (switching speed) the dc consumption increases. The front-end printed circuit board (PCB) was fabricated using inkjet

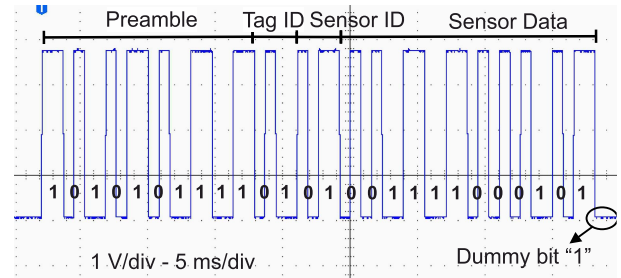


Fig. 7. Example of the oscilloscope-measured transmitted rectangular pulses (MCU output). The packet (“bit stream”) consists of the Preamble, Tag ID, Sensor ID and Sensor Data bits, and an extra dummy bit “1” at the end.

printing technology on a paper substrate. The characteristics of the the substrate was:  $\epsilon_r = 2.9$ ,  $\tan \delta = 0.045$ , and substrate height 210  $\mu\text{m}$ . The traces were printed with conductive silver nanoparticle ink and conductive epoxy deposition was used in order to attach the switch to the substrate.

In order to minimize the average power consumption, a duty cycle operation was programmed where the tag was active only for a desired minimum period of time. The duty cycle operation was set using the RTC and the sleep mode of the MCU. A future challenge for the tag is to employ RF harvesters and solar cells for powering as it is shown in [17] and [18].

### B. Telecommunication Protocol

The tag uses amplitude-shift keying (ASK) modulation to transmit its data via backscattering. More specifically, by changing the RF switch states between “ON” and “OFF” and backscattering the ambient FM broadband signals, a binary ASK modulated signal of OOK type can be created and described by (5). Using OOK modulation, the information-containing received tag signal of (5) can be expressed as [12]

$$\Gamma(t - \tau_{\text{TR}}) = \sum_{n=0}^{N-1} x_n \Pi[t - nT_{\text{symbol}} - \tau_{\text{TR}}] \quad (7)$$

where  $x_n \in \{-1, 1\}$  are the  $N$  transmitted symbols and  $\Pi(t)$  is the pulse (symbol) with duration  $T_{\text{symbol}}$ . In addition to the OOK modulation, the low-power consuming FM0 technique is utilized to encode the sensor data. For binary OOK,  $x_n$  would be the bits and for FM0-coded OOK,  $x_n$  are the binary symbols. In FM0 encoding, there is an inversion of the phase at every bit boundary (at the beginning and at the end of every bit), and additionally bit “0” has an additional phase inversion in the middle [Fig. 6 (left)]. Each bit includes two symbols, as shown in Fig. 6. The duration of a bit and of a symbol are denoted as  $T_{\text{bit}}$  and  $T_{\text{symbol}}$ , respectively. The data bit rate is  $1/T_{\text{bit}}$  bit/s. The FM0 encoding always ends with a dummy “1” bit in order to detect easily the end of the bitstream. In the case that the received backscatter waveform finishes with a “LOW,” it would be indistinguishable from receiving the reader’s CW only (i.e., no packet transmission).

The tag is programmed to send the data in packets to the reader and the reader tries to receive and decode them. The length of each packet is fixed. Fig. 7 shows a typical packet format. The packet has the length of 26 b and begins with the

preamble bits. After that follow the “Tag ID” bits, the “Sensor ID” bits and finally the “Sensor Data” bits. The preamble is useful for bit-level synchronization at the RX and was fixed to be 1010101111 (10 b) in our proof-of-concept tests. The “Tag ID” (2 b) is utilized in the case of simultaneous multiple tag utilization. As mentioned before, the tag can support up to four sensors, and therefore the “Sensor ID” (2 b) is used to identify the sensor the data is coming from.

#### IV. RECEIVER THEORY

In this paper, ambient backscatter modulation based on OOK modulation with FM0 encoding is used, as in conventional passive RFID tags [19]. An example of FM0 encoding is shown in Fig. 6 (left). As a result, four possible waveforms are transmitted corresponding to a 2-D bi-orthogonal constellation. However, if one observes the FM0 signal shifted by one symbol, only two possible waveforms exist, which are the ones of bit “0.” These two waveforms correspond to a 1-D antipodal constellation which is easier to study and decode [20]. The detected bits from the half-bit time shifted signal correspond to the originally transmitted bits after differential encoding. Therefore, one can proceed to decode the FM0 signal in two steps, first detecting the time-shifted bits and then using a differential decoder to recover the originally transmitted bits. In this section, we first derive the error probability  $P_s$  of the time shifted signal. Once  $P_s$  is obtained, the error probability of the originally transmitted bit stream  $P_e$  is given in [20] and [21]

$$P_e = 2P_s(1 - P_s). \quad (8)$$

As it is shown in [20], in addition to the simplification of the detection process, the fact that an antipodal constellation is used leads to an SNR improvement of approximately 3 dB in comparison to the standard detection method based on the bi-orthogonal constellation.

In order to derive  $P_s$ , one may proceed following [12] and [22]. In [12], a thorough analysis of traditional backscattering in a bi-static configuration is presented using a CW carrier signal. OOK modulation was assumed but without considering FM0 encoding. In [22], the analysis of the error probability of ambient backscatter systems was presented considering randomly modulated signals. In addition the special case of phase shift-keying modulation is treated in Appendix B, which is similar in analysis to FM signals used in this paper, in that the carrier amplitude is constant. However, Qian *et al.* [22] also does not use FM0 encoding. In this paper, we proceed by following the formulation of [22] but treat the case of FM0 encoding taking into account [20] as described in the previous paragraph. The received signal complex envelope was given in (5) and repeated here for convenience in a more compact form

$$y(t) = Ae^{-jD}(\alpha_1(t)e^{-jK_1} + \alpha_2(t)b(t)e^{-jK_2}) + n(t). \quad (9)$$

The term  $D$  includes the frequency and phase offset,  $K_1$  is the delayed modulation signal arriving directly from TX to the RX and  $K_2$  delayed modulation signal arriving through the tag.  $b(t)$  is the information signal and  $n(t)$  is additive

zero mean complex white Gaussian noise added at the RX  $n(t) \sim \mathcal{N}(0, N_w)$ . Following [22], we assume that  $K_1 = K_2$  due to the fact that the two paths are approximately equal. In addition, any thermal noise generated in the tag is ignored as very low [22] value. The obtained equation is

$$y(t) \approx Ae^{-jD}e^{jK}h(t) + n(t) \quad (10)$$

where  $h(t) = a_1(t) + a_2(t)b(t)$  is the complex valued signal containing the information from the tag and the channel effects. In order to eliminate the frequency and phase offset in the RX, we form the magnitude square of the envelope

$$\begin{aligned} Z(t) &= A^2|h(t)|^2 + |n(t)|^2 + 2\Re\{Ae^{-jD}e^{jK}h(t)n^*(t)\} \\ &= A^2|h(t)|^2 + w(t). \end{aligned} \quad (11)$$

Following [22, Appendix B], and invoking the central limit theorem (CLT),  $w(t)$  is a real Gaussian process with mean and variance given by

$$w(t) \sim \mathcal{N}(N_w, N_w^2 + 2A^2N_w|h(t)|^2). \quad (12)$$

The  $N_w$  is the noise power at the RX. One should note that before the decoding process the RX applies a low pass filter consisting of an averaging operation of approximately 1000 samples, which further supports the reasoning of invoking the CLT. The RX applies a synchronization algorithm to derive the beginning of the information signal which is described in more detail in Section V. In order to facilitate the synchronization process a dc offset removal was applied to  $Z(t)$ . Due to the fact that the dc offset removal does not affect the detection process it will not be considered in this section. Once synchronization is achieved a time shifted version of the received bits  $Z(t)$  is considered and detection based on an antipodal constellation is applied. Specifically, the received signal  $Z(t)$  is correlated with pulse

$$q(t) = \begin{cases} +1, & \text{if } 0 < t \leq \frac{T_{\text{bit}}}{2} \\ -1, & \text{if } \frac{T_{\text{bit}}}{2} < t \leq T_{\text{bit}} \end{cases} \quad (13)$$

giving

$$U(t) = X + V = \int_0^{T_{\text{bit}}} A^2|h(t)|^2q(t)dt + \int_0^{T_{\text{bit}}} w(t)q(t)dt. \quad (14)$$

Due to binary modulation  $|h(t)|^2$  takes one of two values  $|h_H|^2$  or  $|h_L|^2$ . It is straightforward to show that  $V$  is a real gaussian process with mean and variance given by

$$V \sim \mathcal{N}(0, 2T_{\text{bit}}N_w^2 + T_{\text{bit}}A^2N_w(|h_H|^2 + |h_L|^2)). \quad (15)$$

Similarly,

$$X_{\pm} = \pm \frac{T_{\text{bit}}}{2} A^2(|h_H|^2 - |h_L|^2) \quad (16)$$

with the sign depending on whether  $q(t)$  or  $-q(t)$  was transmitted. Assuming equal probability of transmission of the two possible symbols, one derives

$$P_s = P\{U < 0|+\} = Q\left(\frac{X_+}{\sigma_V}\right) \quad (17)$$

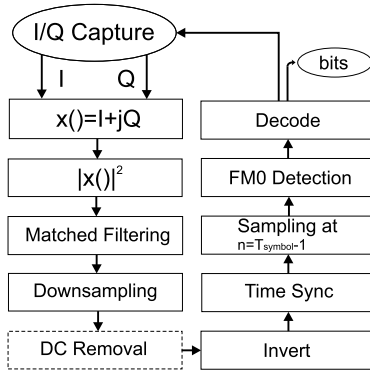


Fig. 8. Flowchart of the real-time RX algorithm.

where  $Q(x)$  is the tail probability of the normal distribution function [20], [21].  $P(U < 0|+)$  denotes the probability that  $U < 0$  when  $q(t)$  was transmitted. Therefore, the originally transmitted bit error probability is

$$P_e = 2Q\left(\frac{X_+}{\sigma_V}\right) \left(1 - Q\left(\frac{X_+}{\sigma_V}\right)\right). \quad (18)$$

It should be noted that in order to compute  $P_e$  one needs information of the signal at the two different states  $|h_H|^2$  and  $|h_L|^2$  but also of the noise power  $N_w$ , something which was also highlighted in [22, Appendix B].

A method to compute  $P_e$  is outlined in order to compare the theoretical analysis with bit-error rate measurements. Consider a given setup of TX, tag and RX, and perform the following three power measurements, i.e., on signal  $Z(t)$ . While transmitting a modulated signal, set the tag to a fixed state and measure the received power, to obtain

$$P_{yH} = A^2|h_H|^2 + N_w \quad (19)$$

and

$$P_{yL} = A^2|h_L|^2 + N_w. \quad (20)$$

Then turn the TX OFF and measure the noise power  $N_w$ . The most significant noise contribution is due to the RX electronics and thus the state of the tag during the noise measurement is not important. Using the three measurements one has

$$X_{\pm} = \pm \frac{LT_s}{2}(P_{yH} - P_{yL}) \quad (21)$$

and

$$\sigma_V^2 = LT_s N_w (P_{yH} + P_{yL}) \quad (22)$$

where  $T_s$  is the sampling period. In our implementation  $L = 10$  samples per bit were used. Using the  $P_{yH}$ ,  $P_{yL}$  and  $N_w$  measurements, one can apply (21) and (22) in (18) to compute the theoretical BER for a given TX power level.

## V. RECEIVER IMPLEMENTATION

### A. SDR

In this paper, the low cost (22 USD) RTL SDR (Noelec NESDR SMart) was used as RX. It is an improved version of RTL SDR dongle that was used in [9] and [23], and it is based on the same RTL2832U demodulator/USB interface

IC and R820T2 tuner. The new version provides a better oscillator, temperature stability and antenna improvements compared to the old one. It comes with an ultralow phase noise 0.5 PPM temperature compensated crystal oscillator (Phase noise @100 kHz:  $-152$  dBc/Hz). The dongle was redesigned with an RF-suitable voltage regulator with under  $10 \mu\text{VRMS}$  of noise for lower power consumption. Power consumption has been reduced by an average of 10 mA according to manufacturer [24]. A custom heatsink is affixed to the primary PCB for temperature improvement and it comes with a low-loss RG58 feed cable and SMA antenna connector for better signal reception. In general the RTL SDR has a tuning frequency range from 24 to 1850 MHz and it can support sampling rates up to 2.8 MS/s. The SDR downconverts the received RF signal to baseband and sends in-phase (I) and quadrature (Q) samples to the PC through the USB interface, while it is connected to an improved telescopic monopole antenna in order to receive the FM signals.

### B. Receiver Algorithm

The received signal of (5) contains the useful bits in FM0 encoding [rectangular pulses in (7)]. A real-time RX and digital signal processing was implemented in order to read the backscattered information sent from the tag. The steps of the algorithm are briefly shown in Fig. 8 and the software that was used was MATLAB and GNU radio framework. The GNU radio provides the I and Q samples to MATLAB through a FIFO file and the samples are interleaved for further processing. The received digitized signal after sampling with a sampling period  $T_s$ , can be written as

$$y_r[k] = y_{\text{amb}}(kT_s + \tau_{TR}) = x_r[k] + n[k] = I[k] + jQ[k] \quad (23)$$

with  $n[k] = n(kT_s)$  and  $n[k] \sim \mathcal{N}(0, \sigma_n^2)$ . The term  $x_r[k]$  is the signal without noise that consists of a dc component, a modulated component and the ambient FM signal utilized for the backscattering. The algorithm collects and process the data in a window with duration:  $3 \times$  packet duration.

The first step of the signal processing algorithm is the CFO correction. In our case, CFO is the frequency difference between the FM, TX, and SDR reader and, if not properly removed it causes a performance loss at the RX. In order to eliminate this term without using an *a priori* CFO estimation and correction algorithm, the absolute value  $|y_r[t]|^2$  was taken, which is an established CFO compensation technique in digital communication textbooks, such as [25].

A matched filter was then applied to the samples in order to filter out noise and interference terms and maximize the SNR, consisting of a square pulse with duration  $T_{\text{symbol}}$ . Fig. 9 (top) depicts the received packet of Fig. 7 after absolute square operation. The same packet after matched filtering is shown in Fig. 9 (bottom). Matched filtering was followed by downsampling by a factor of 10 in order to reduce the computational cost of the subsequent operations without compromising the detection quality.

The dc offset of the received window was estimated by averaging some samples when the tag is not transmitting data

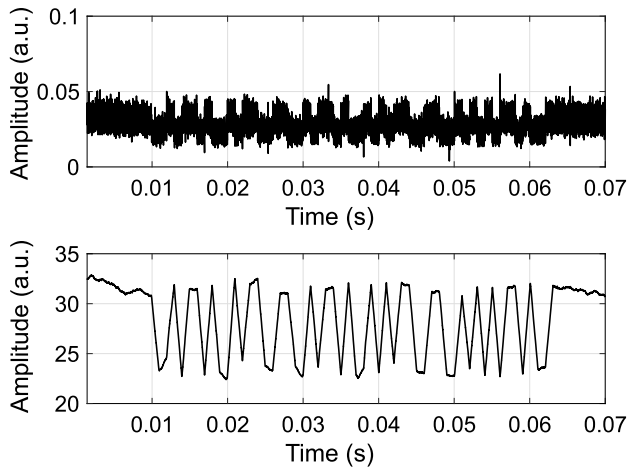


Fig. 9. Received signal including a data packet. Squared absolute value signal (top). Received signal after matched filtering for a symbol period,  $T_{\text{symbol}} = 1$  ms (bottom). The packet is flipped due to the channel characteristics.

(average at the start or at the end of the window). The dc offset was removed by subtracting the above estimate from all the values within the receive window. The outcome of this step can be an upright or an inverted waveform. In the case shown in Fig. 9 (bottom), an inverted waveform will result after the dc offset removal. Upright or inverted waveforms may result due to the channel propagation characteristics. If an inverted waveform is detected after the dc offset removal, it is flipped so that only upright waveforms  $y_{fl}$  are forwarded to the synchronization block.

The received signal must be symbol-synchronized in order to determine when the packet starts. In order to find the starting sample of the packet, cross correlation with the known preamble symbol sequence (11010010110100110011) was used. The similarity of the waveform  $y_{fl}$  and the preamble sequence  $p$  was evaluated as a function of the time-lag according to

$$C[n] = \sum_{t=1}^{\infty} p[t]y_{fl}[t+n], \quad n \in [0, N_s/2] \quad (24)$$

with  $N_s$  the number of received packet samples. The starting point of the packet is defined as

$$I_{\text{start}}[n] = \arg \max_n C \quad (25)$$

which corresponds to the position of the peak of the cross correlation between the known sequence  $p$  and the received waveform.

In FM0-encoded signals, the received bits can be determined by comparing two neighboring symbols. In order to begin decoding,  $y_{fl}[t]$  is shifted to sample  $I_{\text{start}} + P - T_{\text{symbol}}$ , where  $P$  is the length of the preamble. Two possible orthogonal pulse waveforms can be received, as shown in [20] and used in [26]. The two waveforms are indicated in Fig. 6 (right) with a solid line square and a dashed line square. With this observation the algorithm has to easily decode two adjacent received symbols in order to detect a whole bit. This method gives a gain of 3 dB compared to maximum likelihood symbol-by-symbol detection [27]. The two orthogonal waveforms can

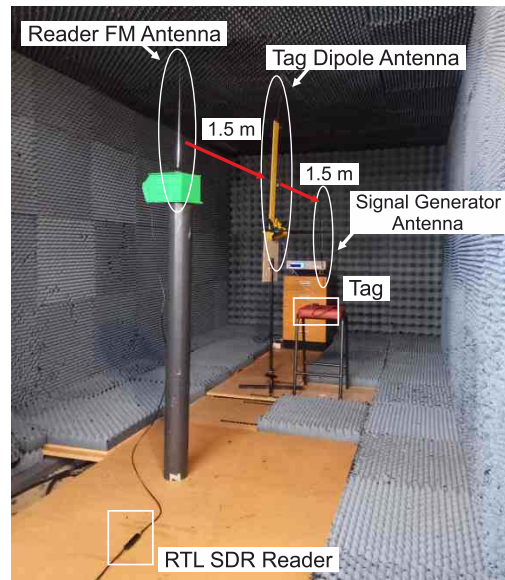


Fig. 10. Anechoic chamber experimental setup. The RX antenna was placed at 1.5 m away from the tag and the tag was placed at 1.5 m away from the signal generator.

be expressed as

$$D_1[k] = \begin{cases} +1, & \text{if } 0 < k \leq \frac{M}{2} \\ -1, & \text{if } \frac{M}{2} < k \leq M \end{cases} \quad (26)$$

and  $D_2[k] = -D_1[k]$  with  $M$  the oversampling factor  $T_{\text{symbol}}/T_s$ . The shifted signal is correlated with  $D_1[k]$  and  $D_2[k]$  and it is possible to determine which bit has been sent according to [28]

$$S_k = \begin{cases} 1, & \text{if } \sum_{i=1}^{N_s} y_{\text{sh}}[i]D_1[i] > \sum_{i=1}^{N_s} y_{\text{sh}}[i]D_2[i] \\ 0, & \text{elsewhere} \end{cases} \quad (27)$$

with  $y_{\text{sh}}[t]$  is the shifted version of waveform  $y_{fl}[t]$ . The results from the above calculation were stored in a vector  $L$  and the estimated bit  $a_{k+1}$  that was sent is determined by

$$a_{k+1} = \begin{cases} 0, & \text{if } L_k = L_{k+1} \\ 1, & \text{elsewhere.} \end{cases} \quad (28)$$

It is noticed that the first waveform derived by this decoding procedure is from the last preamble symbol [decoding starting point in Fig. 6 (right)]. The following waveforms will be either  $D_1$  or  $D_2$ . This means that if the first waveform is  $D_1$  and the second is  $D_2$  and vice versa, the bit “1” was sent, otherwise the bit “0” was transmitted.

## VI. EXPERIMENTAL RESULTS

In this paper, we tried to produce a systematic set of measurements and compare them with the theoretical result of (18). For the systematic characterization in a controlled environment the system was demonstrated first in the anechoic chamber of the Heriot-Watt Microwaves and Antennas Laboratory (Fig. 10). The tag was placed in a far-field anechoic

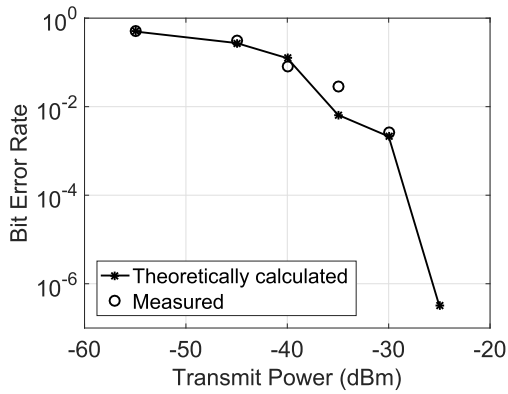


Fig. 11. Measured and theoretically calculated BER versus the signal generator transmit power for 0.5 kb/s.

chamber together with an analog signal generator used as a TX. The SDR RX was also placed at the edge of the anechoic chamber. The tag, TX and RX are in fixed locations with fixed distances tag-TX 1.5 m and tag-RX 1.5 m. The TX and RX use commercial passive FM antennas with gain 2.5 dBi while the tag antenna is a wire dipole. The anechoic chamber was not specified to work at FM frequencies, but it was used to minimize multipath and external interference.

The analog signal generator produces an FM modulated signal with a carrier centered at 98.5 MHz and frequency deviation of 75 kHz. The carrier frequency was selected so as to utilize a frequency band without any interference from any external stations. We used a sinusoidal signal with a frequency of 15 kHz to modulate the TX carrier. The 15 kHz is equal to the end of mono audio (left and right) signal frequency of a standard stereo FM signal transmission (Fig. 3) and that FM stations typically use a 75-kHz deviation [13].

The tag was programmed to send packets with fixed information bits for bit rate: 500 bit/s. An oscilloscope measurement of the packet transmitted at 500 bit/s is presented in Fig. 7. The data information was the 12-bit binary representation of 965 mV: 001111000101.

The RX has a bandwidth of 1 MHz around the carrier frequency. The noise power  $P_w$  at the RX was computed over the 1-MHz bandwidth while TX was OFF. Then, for a given transmit power at the TX, the received power at RX was recorded while the tag was set to a fixed load state  $A$  or  $B$ , resulting in  $P_{yH}$  or  $P_{yL}$ . The measured data consist of downconverted time domain values, which were converted in the frequency domain by taking a fast Fourier transform (FFT) and the total power was computed by taking the sum of the squared magnitude values of the FFT operation. It is noted that  $P_{yH}$  and  $P_{yL}$  correspond to the total signal plus noise power measurement. Two sets of  $P_{yH}$  and  $P_{yL}$  measurements were collected for a varying transmit power from  $-55$  to  $-25$  dBm. In order to compute an estimate of average power values, for each transmit power, 200 sets of data were collected and an average power value was computed.

The BER was measured for each value of the transmitted power while the tag rate was backscattering a fixed package with bit rate of 500 bit/s. In addition, the BER was recorded for each transmit power level. The resulting BER versus

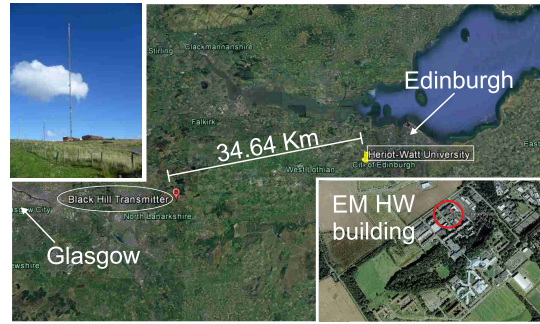


Fig. 12. Scotland FM radio outdoor deployment. The BBC 95.8-MHz station in “Radio 2” band was selected for measurements. The FM transmitter was 34.5 km away from the measurement’s setup and its transmission power was 250 kW.

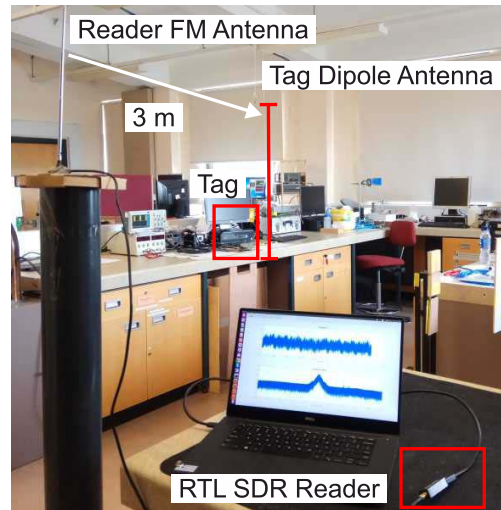


Fig. 13. Indoor experimental setup. The tag with the FM dipole antenna was set in a vertical position and the RX was tuned at the most powerful FM station. For communication measurements, the RX was placed at a maximum of 5 m away from the tag with the RX antenna on top of a beam.

TX transmit power curves are shown in Fig. 11 along with the theoretical BER results ( $P_e$ ). To calculate the analytical BER, the measured values of  $P_{yH}$  and  $P_{yL}$  and  $N_w$  were used with (18). One can see a good agreement between simulation and measurement. BER measurements were performed for transmitted power levels up to  $-30$  dBm where the BER approached  $10^{-3}$ . Due our system memory limitations it was not possible to setup longer measurements containing a sufficient number of data to ensure a good confidence level of BER measurements. The equation that can be rearranged to calculate the number of bits required for a given BER and confidence level ( $C_L$ ) is [29]

$$N_{\text{bits}} = \frac{-\ln(1 - C_L)}{\text{BER}}. \quad (29)$$

For example, for a typical confidence level of 0.95, the required number of bits to test without any errors is  $2.99573 \times 10^7$  in comparison to our case that we had only 9616 transmitted bits.

The proposed system was also tested indoors in the Heriot-Watt Microwaves and Antennas Laboratory, selecting the most powerful FM station as the ambient RF source

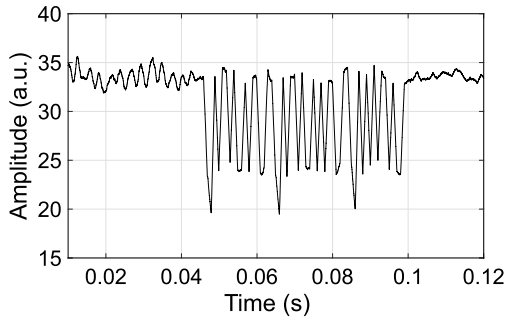


Fig. 14. Corrected received packet after matched filtering at  $T_{\text{symbol}} = 1$  ms (500 bit/s) featuring a smaller channel fluctuation. High frequency noise components can be observed.

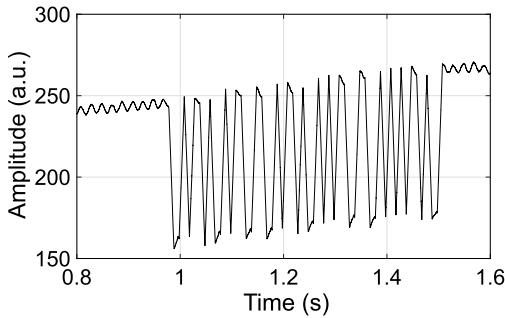


Fig. 15. Corrected received packet after matched filtering for  $T_{\text{symbol}} = 10$  ms (50 bit/s) including the channel fluctuation effects. A better filtering quality is observed.

to use in backscattering. Thus, the RX was tuned to BBC 95.8-MHz station with 1-MS/s sampling rate. The station is located 34.5 Km away at the “Black Hill” location between the town of Edinburgh and Glasgow as depicted in Fig. 12. The transmission power of the station is 250 kW. The power of the FM station carrier signal was measured in the vicinity of the tag antenna in the laboratory at  $-51$  dBm. The reader was placed close to the tag at different reader-to-tag distances with a maximum range of 5 m (Fig. 13). The antenna of the reader was placed on top of a plastic stick with height 1.5 m for better reception.

The tag was programmed to send packets with the fixed information bits (same as above) for the following different bit rates: 50, 100, 500, 1000, 1250, and 2500 bit/s. The received packets for 500 and 50 bit/s after the matched filtering step are illustrated in Figs. 14 and 15, respectively. One can see that the packets are inverted due to the channel conditions, i.e., random, unknown channel phase. It is clear that there is tradeoff between bit rate and efficient filtering. In case that a high-bit rate is employed (Fig. 14), there is less channel fluctuation, and the matched filtering operation is not able to remove the high-frequency components of the ambient FM signal, due to the wider bandwidth of the matched filter. In the case of low-bit rate transmission (Fig. 15) the filtering operation is more effective, corresponding to a higher SNR, but a channel fluctuation effect is visible. When channel fluctuation is present it is more difficult to decode the packet due to the fast varying signal level.

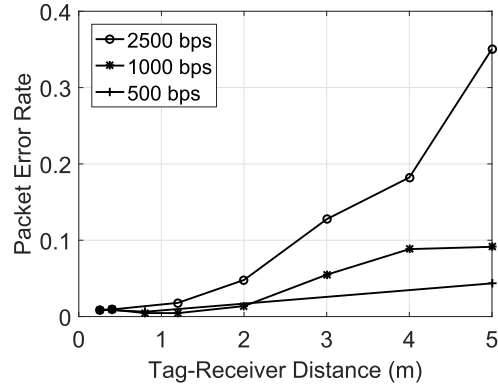


Fig. 16. Measured PER versus the tag-RX distance for 0.5, 1, and 2.5 kb/s.

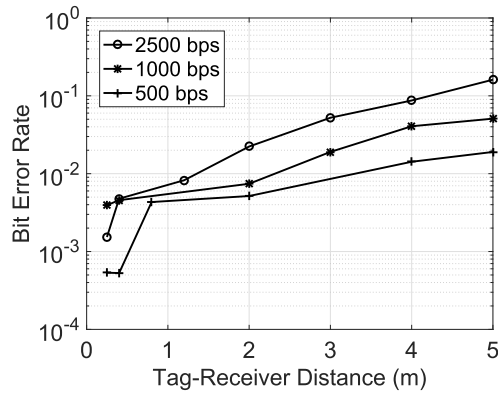


Fig. 17. Measured BER versus the tag-RX distance for 0.5, 1, and 2.5 kb/s.

In order to validate the effectiveness of our digital backscatter communication system, numerous range measurements were performed indoors with the setup described above. Figs. 16 and 17 display the BER and PER performance as a function of the tag-to-reader distance for the three different data rates. The minimum PER and BER value at 5 m was measured to be 0.043 and 0.0019, respectively. As the tag-to-RX distance decreases, the reader can decode successfully more the bit packets. It is also seen that for a given distance value, reducing the bit rate improves the PER and BER performance. However, transmitting packets at lower bit rates result in increased transmission time and energy per packet while the MCU and the front-end staying in “ON” state for longer time. There is a direct and inversely proportional relationship between the bit rate and the energy that a tag consumes sending a packet as shown in Table I, where the energy per packet for 6-bit rates is presented. The table also provides the tag power consumption for each bit rate. A higher power consumption of the MCU electronics is observed when operating at a higher bit rate. In order to compile the measurements shown in Table I, the tag was programmed to wake up every 3 s, transmit a packet and go to sleep mode, while being powered from the supercapacitor.

The power consumption of the tag can be reduced by the following modifications which are the object of future work. First, it is possible to use a more energy efficient MCU such as PIC16LF1459 ( $25 \mu\text{A}/\text{MHz}$  at 1.8 V) [30]. Similarly, one can select sensing elements with minimum power dissipation

TABLE I  
TAG POWER CHARACTERISTICS

| Bit Rate (bps) | Power (mW) | Energy/Packet ( $\mu$ J) |
|----------------|------------|--------------------------|
| 2500           | 2.838      | 36.9                     |
| 1250           | 2.087      | 43.4                     |
| 1000           | 1.785      | 46.4                     |
| 500            | 1.283      | 66.73                    |
| 100            | 0.751      | 195.45                   |
| 50             | 0.677      | 352.15                   |

or even employ some passive sensing technique such as [31] and [32]. Second, the RF front-end can be modified to use instead of an off-the-shelf switch, a single transistor-based switch such as the ones in [33] and [34] with pJ/bit energy consumption. Finally, a customized CMOS-based IC may provide an even further reduction of dissipated power, as suggested in [6]. In addition to reducing the circuit consumption, battery-less operation can be achieved by exploring energy harvesting techniques. There are several studies related to the availability of ambient RF energy [35]–[38] as well as demonstrations of sensors powered by harvesting ambient RF energy from TV [18], WiFi [39], or even microwave oven signals [40], which could be used for smart house-targeted sensors. In addition, multiple technology of energy harvesters such as solar and electromagnetic energy harvesters can be employed in order to combine the different forms of ambient energy availability [17], [41].

Finally, the potential interfering effects of ambient backscatter systems on the performance of the ambient systems it utilizes should be considered. In U.S.A., according to the Federal Communications Commission (FCC), it is illegal to broadcast unlicensed signals on FM band (88 to 108 MHz) [42]. However, devices that communicate with backscatter signals (e.g., RFID tags) have not been reviewed by FCC. The reason is that the RF front ends of backscatter tags are not active components (have no amplifiers) and they only modulate the reflections of the incoming signals. Consequently the power of the reflected signals is of very low levels. The ambient backscatter operation such as our developed system belongs to the category of RFID tags so it is not illegal under current rules. However, the reflected signals of existing FM signals could interfere with commercial FM RXs. In the Heriot-Watt Microwaves and Antennas laboratory, an FM-RX equipped smartphone was tested in the worst case interference scenario, where random data was continuously backscattered. The received audio quality was practically unchanged when the backscatter tag was placed right at the vicinity of the smartphone. This is only a simple experiment, and a detailed experimental study is required to determine the level and limits of interference generated by ambient backscatter systems which represents the object of future work.

## VII. CONCLUSION

In this paper, we presented a novel FM backscatter tag and RX system. The tag communicates with a low cost SDR reader by backscattering the ambient FM signals. Data acquisition from sensors with low power operation and communication ranges up to 5 m has been demonstrated experimentally. The communication was implemented with OOK modulation over

the modulated carrier of the most powerful FM station. This concept can be the next novel way for low power and low cost long range communication.

## ACKNOWLEDGMENT

The authors would like to thank R. Joshi and all members of Agile Technologies for High-frequency Electromagnetic Applications (ATHENA) Group, Georgia Institute of Technology, Atlanta, GA, USA, for their help in various steps throughout this paper. Authors S. N. Daskalakis and A. Georgiadis would like to thank LRF and ICON.

## REFERENCES

- [1] W. Liu, K. Huang, X. Zhou, and S. Durrani, "Next generation backscatter communication: Theory and applications," *CoRR*, vol. abs/1701.07588, no. 229, Jan. 2017.
- [2] H. Stockman, "Communication by means of reflected power," *Proc. IRE*, vol. 36, no. 10, pp. 1196–1204, Oct. 1948.
- [3] A. P. Sample, D. J. Yeager, P. S. Powlledge, A. V. Mamishev, and J. R. Smith, "Design of an RFID-based battery-free programmable sensing platform," *IEEE Trans. Instrum. Meas.*, vol. 57, no. 11, pp. 2608–2615, Nov. 2008.
- [4] S. Naderiparizi, A. N. Parks, Z. Kapetanovic, B. Ransford, and J. R. Smith, "WISPCam: A battery-free RFID camera," in *Proc. IEEE Int. Conf. RFID*, Apr. 2015, pp. 166–173.
- [5] V. Liu, A. Parks, V. Talla, S. Gollakota, D. Wetherall, and J. R. Smith, "Ambient backscatter: Wireless communication out of thin air," *ACM SIGCOMM Comput. Commun. Rev.*, vol. 43, no. 4, pp. 39–50, Sep. 2013.
- [6] A. Wang, V. Iyer, V. Talla, J. R. Smith, and S. Gollakota, "FM backscatter: Enabling connected cities and smart fabrics," in *Proc. USENIX Symp. Netw. Syst. Design Implement. (NSDI)*, Boston, MA, USA, Mar. 2017, pp. 243–258.
- [7] B. Kellogg, A. Parks, S. Gollakota, J. R. Smith, and D. Wetherall, "Wi-Fi backscatter: Internet connectivity for RF-powered devices," in *Proc. ACM Conf. (SIGCOMM)*, Chicago, IL, USA, Aug. 2014, pp. 607–618.
- [8] D. Bharadia, K. R. Joshi, M. Kotaru, and S. Katti, "BackFi: High throughput WiFi backscatter," in *Proc. ACM Conf. (SIGCOMM)*, London, U.K., Aug. 2015, pp. 283–296.
- [9] S. N. Daskalakis, J. Kimionis, A. Collado, M. M. Tentzeris, and A. Georgiadis, "Ambient FM backscattering for smart agricultural monitoring," in *IEEE MTT-S Int. Microw. Symp. Dig.*, Honolulu, HI, USA, Jun. 2017, pp. 1339–1341.
- [10] V. Palazzari, P. Mezzanotte, F. Alimenti, F. Fratini, G. Orecchini, and L. Roselli, "Leaf compatible 'eco-friendly' temperature sensor clip for high density monitoring wireless networks," *Wireless Power Transf.*, vol. 4, no. 1, pp. 55–60, Feb. 2017.
- [11] K. Kurokawa, "Power waves and the scattering matrix," *IEEE Trans. Microw. Theory Techn.*, vol. MTT-13, no. 2, pp. 194–202, Mar. 1965.
- [12] J. Kimionis, A. Bletsas, and J. N. Sahalos, "Increased range bistatic scatter radio," *IEEE Trans. Commun.*, vol. 62, no. 3, pp. 1091–1104, Mar. 2014.
- [13] L. Der, "Frequency modulation FM tutorial," Silicon Lab. Inc., Austin, TX, USA, Tech. Rep., 2008. [Online]. Available: <https://www.silabs.com/Marcom%20Documents/Resources/FMTutorial.pdf>
- [14] Texas Instruments. (2015). *MSP430FR5969 LaunchPad Development Kit, Product Manual*. [Online]. Available: <http://www.ti.com/lit/ug/slau535b/slau535b.pdf>
- [15] Analog Devices. (2005). *ADG902 RF Switch, Product Manual*. [Online]. Available: [http://www.analog.com/media/en/technical-documentation/data-sheets/ADG901\\_902.pdf](http://www.analog.com/media/en/technical-documentation/data-sheets/ADG901_902.pdf)
- [16] S. J. Thomas and M. S. Reynolds, "A 96 Mbit/sec, 15.5 pJ/bit 16-QAM modulator for UHF backscatter communication," in *Proc. IEEE Int. Conf. RFID*, Orlando, FL, USA, Apr. 2012, pp. 185–190.
- [17] K. Niotaki, A. Collado, A. Georgiadis, S. Kim, and M. M. Tentzeris, "Solar/electromagnetic energy harvesting and wireless power transmission," *Proc. IEEE*, vol. 102, no. 11, pp. 1712–1722, Nov. 2014.
- [18] S. Kim *et al.*, "Ambient RF energy-harvesting technologies for self-sustainable standalone wireless sensor platforms," *Proc. IEEE*, vol. 102, no. 11, pp. 1649–1666, Nov. 2014.
- [19] D. M. Dobkin, *The RF in RFID: Passive UHF in Practice*. Burlington, MA, USA: Newnes, 2008.

- [20] M. Simon and D. Divsalar, "Some interesting observations for certain line codes with application to RFID," *IEEE Trans. Commun.*, vol. 54, no. 4, pp. 583–586, Apr. 2006.
- [21] S. G. Wilson, *Digital Modulation and Coding*. Englewood Cliffs, NJ, USA: Prentice-Hall, 1995.
- [22] J. Qian, F. Gao, G. Wang, S. Jin, and H. Zhu, "Noncoherent detections for ambient backscatter system," *IEEE Trans. Wireless Commun.*, vol. 16, no. 3, pp. 1412–1422, Mar. 2017.
- [23] S.-N. Daskalakis, S. D. Assimonis, E. Kampianakis, and A. Bletsas, "Soil moisture scatter radio networking with low power," *IEEE Trans. Microw. Theory Techn.*, vol. 64, no. 7, pp. 2338–2346, Jul. 2016.
- [24] NooElec Inc. (2017). *NESDR SMARt Bundle-Premium RTL-SDR, Product Manual*. [Online]. Available: <http://www.nooelec.com/store/nesdr-smart.html>
- [25] J. G. Proakis, *Digital Communications*, 4th ed. New York, NY, USA: McGraw-Hill, 1998.
- [26] A. Bletsas, J. Kimionis, A. G. Dimitriou, and G. N. Karystinos, "Single-antenna coherent detection of collided FM0 RFID signals," *IEEE Trans. Commun.*, vol. 60, no. 3, pp. 756–766, Mar. 2012.
- [27] N. Kargas, F. Mavromatis, and A. Bletsas, "Fully-coherent reader with commodity SDR for Gen2 FM0 and computational RFID," *IEEE Wireless Commun. Lett.*, vol. 4, no. 6, pp. 617–620, Dec. 2015.
- [28] M. Bamiedakis-Pananos, "Synchronization and detection for Gen2 RFID signals," M.S. thesis, School Elect. Comput. Eng., Tech. Univ. Crete, Chania, Greece, 2015.
- [29] Agilent Technol. Inc. (2006). *Agilent Serial BERT N4901 User's Guide*. [Online]. Available <http://literature.cdn.keysight.com/litweb/pdf/N4901-91030.pdf>
- [30] Microchip Technology Inc. 2014. *PIC16LF1459 USB Microcontroller with Extreme Low-Power Technology, Product Manual*. [Online]. Available: <http://www.microchip.com/downloads/en/DeviceDoc/40001639B.pdf>
- [31] S. Kim, Y. Kawahara, A. Georgiadis, A. Collado, and M. M. Tentzeris, "Low-cost inkjet-printed fully passive RFID tags using metamaterial-inspired antennas for capacitive sensing applications," in *IEEE MTT-S Int. Microw. Symp. Dig.*, Seattle, WA, USA, Jun. 2013, pp. 1–4.
- [32] R. Bhattacharyya, C. Floerkemeier, and S. Sarma, "Low-cost, ubiquitous RFID-tag-antenna-based sensing," *Proc. IEEE*, vol. 98, no. 9, pp. 1593–1600, Sep. 2010.
- [33] R. Correia, A. Boaventura, and N. B. Carvalho, "Quadrature amplitude backscatter modulator for passive wireless sensors in IoT applications," *IEEE Trans. Microw. Theory Techn.*, vol. 65, no. 4, pp. 1103–1110, Apr. 2017.
- [34] J. Kimionis and M. M. Tentzeris, "Pulse shaping: The missing piece of backscatter radio and RFID," *IEEE Trans. Microw. Theory Techn.*, vol. 64, no. 12, pp. 4774–4788, Nov. 2016.
- [35] H. J. Visser, A. C. F. Reniers, and J. A. C. Theeuwes, "Ambient RF energy scavenging: GSM and WLAN power density measurements," in *Proc. IEEE Eur. Microw. Conf. (EuMC)*, Amsterdam, The Netherlands, Oct. 2008, pp. 721–724.
- [36] L. Guenda, E. Santana, A. Collado, K. Niotaki, N. B. Carvalho, and A. Georgiadis, "Electromagnetic energy harvesting—Global information database," *Trans. Emerg. Telecommun. Technol.*, vol. 25, no. 1, pp. 56–63, Jun. 2014.
- [37] M. Pinuela, P. D. Mitcheson, and S. Lucyszyn, "Ambient RF energy harvesting in urban and semi-urban environments," *IEEE Trans. Microw. Theory Techn.*, vol. 61, no. 7, pp. 2715–2726, Jul. 2013.
- [38] K. Mimis, D. Gibbins, S. Dumanli, and G. T. Watkins, "Ambient RF energy harvesting trial in domestic settings," *IET Microw., Antennas Propag.*, vol. 9, no. 5, pp. 454–462, 2015.
- [39] K. Gudán, S. Chemishkian, J. J. Hull, S. J. Thomas, J. Ensworth, and M. S. Reynolds, "A 2.4 GHz ambient RF energy harvesting system with –20 dBm minimum input power and NiMH battery storage," in *Proc. IEEE Conf. RFID Technol. Appl. (RFID-TA)*, Tampere, Finland, Sep. 2014, pp. 7–12.
- [40] Y. Kawahara, X. Bian, R. Shigeta, R. Vyas, M. M. Tentzeris, and T. Asami, "Power harvesting from microwave oven electromagnetic leakage," in *Proc. ACM Int. Joint Conf. Pervasive Ubiquitous Comput.*, Zurich, Switzerland, Sep. 2013, pp. 373–382.
- [41] J. Bito, R. Bahr, J. G. Hester, S. A. Nauroze, A. Georgiadis, and M. M. Tentzeris, "A novel solar and electromagnetic energy harvesting system with a 3-D printed package for energy efficient Internet-of-Things wireless sensors," *IEEE Trans. Microw. Theory Techn.*, vol. 65, no. 5, pp. 1831–1842, May 2017.
- [42] Federal Communications Commission (FCC). *Permitted Forms Low Power Broadcast Operation, Public Notice 14089*. Accessed: Jul. 1991. [Online]. Available: [https://apps.fcc.gov/edocs\\_public/attachmatch/DOC-297510A1.pdf](https://apps.fcc.gov/edocs_public/attachmatch/DOC-297510A1.pdf)



**Spyridon Nektarios Daskalakis** (S'12) was born in Heraklion, Greece, in 1991. He received the Engineering Diploma (with excellence) and M.Sc. degree in electronic and computer engineering from the Technical University of Crete, Chania, Greece, in 2014 and 2016, respectively. He is currently pursuing the Ph.D. degree at the School of Engineering and Physical Science, Heriot Watt university, Edinburgh, U.K.

He is the Co-Founder of kaloudia.com platform. His current research interests include low-cost wireless sensor networks, RF energy harvesting, backscatter radio communication, batteryless sensors, PCB design, low-cost software-defined radio, environmental sensing, and RF energy harvesting.

Mr. Daskalakis was the recipient of the Fellowship Award for his project Aristeos (olive fly detection and monitoring with wireless sensor network) by Clinton Global Initiative University, Phoenix, AZ, USA, in 2014 and the Onassis Foundation graduate studies 2015/2016 scholarship. He was a recipient for two short-term scientific mission grants from COST Action IC1301 WiPE in electrical and computer engineering, Georgia Institute of Technology, Atlanta, GA, in 2016, and the Centre Tecnològic de Telecomunicacions de Catalunya, Barcelona, Spain, in 2015. He has been a member of the IEEE Microwave Theory and Techniques Society, the IEEE Council on RFID, and the IEEE Sensors Council.



**John Kimionis** (S'10) received the Diploma and M.Sc. degrees in electronic and computer engineering from the Technical University of Crete, Chania, Greece, in 2011 and 2013, respectively. He is currently pursuing the Ph.D. degree at the School of Electrical and Computer Engineering, Georgia Institute of Technology, Atlanta, GA, USA.

He was a Research Assistant with the ATHENA Group in 2017, and a Research Intern with Nokia-Bell Labs, Murray Hill, NJ, USA. His current research interests include spectral-efficient and

energy-efficient backscatter radio and RFID, software-defined radio for sensor networks, RF front-end design for wireless sensors, and additive manufacturing techniques (inkjet and 3-D-printed electronics).

Mr. Kimionis was a recipient of fellowship awards for his undergraduate and graduate studies and has been a Texas Instruments Scholar for his mentoring service for the Opportunity Research Scholars Program of the Georgia Institute of Technology. He was a recipient of the IEEE Student Travel Grants, the First Best Student Paper Award of the IEEE International Conference on RFID-Technologies and Applications (RFID-TA) 2014, Tampere, Finland, the Second Best Student Paper Award of the IEEE International Conference on RFID-TA 2011, Sitges, Barcelona, Spain, and the Third Bell Labs Prize Award 2016 for game-changing technologies on printed electronics and low-cost communications. He has been a member of the IEEE Microwave Theory and Techniques Society and the IEEE Communications Society and is a Board Member of the IEEE MTT-24 RFID Technologies Committee. He currently serves as the Finance Chair of the IEEE International Conference on RFID 2018.



**Ana Collado** (M'08–SM'12) received the M.Sc. and Ph.D. degrees in telecommunications engineering from the University of Cantabria, Santander, Spain, in 2002 and 2007, respectively.

From 2007 to 2016, she was a Senior Research Associate and the Project Management Coordinator with the Technological Telecommunications Center of Catalonia, Barcelona, Spain. Since 2016, she has been an Assistant Professor with the Microwaves and Antennas Research Group, School of Engineering and Physical Sciences, Heriot-Watt University,

Edinburgh, U.K. She has co-authored over 90 papers in journals and conferences. Her current research interests include active antennas, substrate integrated waveguide structures, nonlinear circuit design, and energy harvesting and wireless power transmission solutions for self-sustainable and energy-efficient systems.

Dr. Collado serves on the Editorial Board of the *Radioengineering* journal. She is currently an Associate Editor of *IEEE Microwave Magazine* and the *IET Microwaves, Antennas and Propagation* journal, and an Editorial Board member of the *Cambridge Wireless Power Transfer* journal, *IEEE MTT-26 Wireless Energy Transfer and Conversion*, and *MTT-24 RFID Technologies*. She has participated in national and international research projects. She has collaborated in the organization of several international workshops in different countries of the European Union and a training school for Ph.D. students.



**George Goussetis** (S'99–M'02–SM'12) received the Diploma degree in electrical and computer engineering from the National Technical University of Athens, Athens, Greece, in 1998, the B.Sc. degree in physics (with First Class Honors) from University College London, London, U.K., in 2002, and the Ph.D. degree from the University of Westminster, London, in 2002.

In 1998, he joined the Space Engineering, Rome, Italy, as an RF Engineer, and in 1999, the Wireless Communications Research Group, University of Westminster, London, as a Research Assistant. From 2002 to 2006, he was a Senior Research Fellow with Loughborough University, Loughborough, U.K. He was a Lecturer (Assistant Professor) with Heriot-Watt University, Edinburgh, U.K., from 2006 to 2009, and a Reader (Associate Professor) with Queens University Belfast, Belfast, U.K., from 2009 to 2013. In 2013, he joined Heriot-Watt, as a Reader, and became a Professor in 2014. He has authored or co-authored over 300 peer-reviewed papers, 5 book chapters, and 1 book, and holds 4 patents. His current research interests include microwave and antenna components and subsystems.

Dr. Goussetis held a Research Fellowship from the Onassis Foundation in 2001, a Research Fellowship from the U.K. Royal Academy of Engineering from 2006 to 2011, and a European Marie-Curie Experienced Researcher Fellowship in 2011–2012. He was a co-recipient of the 2011 European Space Agency Young Engineer of the Year Prize, the 2011 EuCAP Best Student Paper Prize, the 2012 EuCAP Best Antenna Theory Paper Prize, and the 2016 Bell Labs Prize. He serves as an Associate Editor for *IEEE ANTENNAS AND WIRELESS PROPAGATION LETTERS*.



**Manos M. Tentzeris** (S'89–M'92–SM'03–F'10) received the Diploma degree (*magna cum laude*) in electrical and computer engineering from the National Technical University of Athens, Athens, Greece, and the M.S. and Ph.D. degrees in electrical engineering and computer science from the University of Michigan, Ann Arbor, MI, USA.

He is currently a Ken Byers Professor in flexible electronics with the School of Electrical and Computer Engineering, Georgia Institute of Technology, Atlanta, GA, USA. He was a Visiting Professor

with the Technical University of Munich, Munich, Germany in 2002, with GTRI-Ireland, Athlone, Ireland, in 2009, and with LAAS-CNRS, Toulouse, France, in 2010. He helped develop academic programs in 3-D/inkjet-printed RF electronics and modules, flexible electronics, origami and morphing electromagnetics, highly integrated/multilayer packaging for RF and wireless applications using ceramic and organic flexible materials, paper-based RFID's and sensors, wireless sensors and biosensors, wearable electronics, "Green" electronics, energy harvesting and wireless power transfer, nanotechnology applications in RF, microwave MEMS, and SOP-integrated (UWB, multiband, mmW, and conformal) antennas. He is the Head of the ATHENA Research Group (20 researchers). He has served as the Head of the GT-ECE Electromagnetics Technical Interest Group, as the Georgia Electronic Design Center Associate Director for RFID/Sensors research, as the Georgia Institute of Technology NSF-Packaging Research Center Associate Director for RF Research, and as the RF Alliance Leader. He has authored more than 650 papers in refereed journals and conference proceedings, 5 books, and 25 book chapters.

Dr. Tentzeris was a recipient/co-recipient of the 2017 Georgia Institute of Technology Outstanding Achievement in Research Program Development Award, the 2016 Bell Labs Award Competition 3rd Prize, the 2015 IET Microwaves, Antennas and Propagation Premium Award, the 2014 Georgia Institute of Technology ECE Distinguished Faculty Achievement Award, the 2014 IEEE RFID-TA Best Student Paper Award, the 2013 IET Microwaves, Antennas and Propagation Premium Award, the 2012 FiDiPro Award in Finland, the iCMG Architecture Award of Excellence, the 2010 IEEE Antennas and Propagation Society Piergiorgio L. E. Uslenghi Letters Prize Paper Award, the 2011 International Workshop on Structural Health Monitoring Best Student Paper Award, the 2010 Georgia Institute of Technology Senior Faculty Outstanding Undergraduate Research Mentor Award, the 2009 IEEE TRANSACTIONS ON COMPONENTS AND PACKAGING TECHNOLOGIES Best Paper Award, the 2009 E. T. S. Walton Award from the Irish Science Foundation, the 2007 IEEE APS Symposium Best Student Paper Award, the 2007 IEEE IMS Third Best Student Paper Award,

the 2007 ISAP 2007 Poster Presentation Award, the 2006 IEEE MTT-S Outstanding Young Engineer Award, the 2006 Asia-Pacific Microwave Conference Award, the 2004 IEEE TRANSACTIONS ON ADVANCED PACKAGING Commendable Paper Award, the 2003 NASA Godfrey "Art" Anzic Collaborative Distinguished Publication Award, the 2003 IBC International Educator of the Year Award, the 2003 IEEE CPMT Outstanding Young Engineer Award, the 2002 International Conference on Microwave and Millimeter-Wave Technology Best Paper Award (Beijing, China), the 2002 Georgia Institute of Technology-ECE Outstanding Junior Faculty Award, the 2001 ACES Conference Best Paper Award, the 2000 NSF CAREER Award, and the 1997 Best Paper Award of the International Hybrid Microelectronics and Packaging Society. He was the TPC Chair of the IEEE MTT-S IMS 2008 Symposium and the Chair of the 2005 IEEE CEM-TD Workshop. He is the Vice-Chair of the RF Technical Committee (TC16) of the IEEE CPMT Society. He is the founder and Chair of the RFID Technical Committee (TC24) of the IEEE MTT-S and the Secretary/Treasurer of the IEEE C-RFID. He is an Associate Editor of the *IEEE TRANSACTIONS ON MICROWAVE THEORY AND TECHNIQUES*, the *IEEE TRANSACTIONS ON ADVANCED PACKAGING*, and the *International Journal on Antennas and Propagation*. He has given more than 100 invited talks to various universities and companies all over the world. He is a member of the URSI-Commission D and the MTT-15 Committee, an Associate Member of EuMA, a Fellow of the Electromagnetic Academy, and a member of the Technical Chamber of Greece. He served as one of the IEEE MTT-S Distinguished Microwave Lecturers from 2010 to 2012 and is one of the IEEE CRFID Distinguished Lecturers.



**Apostolos Georgiadis** (S'94–M'02–SM'08) was born in Salonica, Greece. He received the B.S. degree in physics and M.S. degree in telecommunications from the Aristotle University of Salonica, Salonica, Greece, in 1993 and 1996, respectively, and the Ph.D. degree in electrical engineering from the University of Massachusetts Amherst, MA, USA, in 2002.

In 2002, he joined Global Communications Devices, North Andover, MA, USA, as a Systems Engineer, where he was involved in CMOS transceivers for wireless network applications. In 2003, he joined Bermai Inc., Minnetonka, MN, USA, as an RF/Analog Systems Architect. In 2005, he joined the University of Cantabria, Santander, Spain, as a Juan de la Cierva Fellow Researcher. In 2006, he was a Consultant with Bitwave Semiconductor, Lowell, MA, USA. He collaborated with ACORDE S.A., Santander, where he was involved in the design of integrated CMOS VCOs for ultrawideband applications. In 2007, he joined the Technological Telecommunications Center of Catalonia (CTTC), Barcelona, Spain, as a Senior Researcher of communications subsystems. From 2013 to 2016, he was a Group Leader with the Microwave Systems and Nanotechnology Department, CTTC. In 2016, he joined Heriot-Watt University, Edinburgh, U.K., as an Associate Professor. He has authored more than 180 papers in peer-reviewed journals and international conferences. His current research interests include energy harvesting and wireless power transmission, RFID technology, active antennas and phased-array antennas, inkjet and 3-D printed electronics, and millimeter-wave systems.

Dr. Georgiadis was a recipient of the Fulbright Scholarship for graduate studies at the University of Massachusetts, in 1996. He was the General Chair of the 2011 IEEE RFID-TA Conference and the General Co-Chair of the 2011 IEEE MTT-S IMWS on Millimeter Wave Integration Technologies. He is an EU Marie Curie Global Fellow. He is member of the IEEE MTT-S TC-24 RFID Technologies (past Chair) and a member of the IEEE MTT-S TC-26 Wireless Energy Transfer and Conversion. He was an Associate Editor of the *IET Microwaves Antennas and Propagation* journal, *IEEE MICROWAVE AND WIRELESS COMPONENTS LETTERS*, and the *IEEE RADIO FREQUENCY IDENTIFICATION (RFID) VIRTUAL JOURNAL*. He serves as an Associate Editor for the *IEEE JOURNAL OF RFID* and is the Founder and the Editor-in-Chief of the *Wireless Power Transfer Journal* of Cambridge University Press. He is the Chair of the URSI Commission D, Electronics, and Photonics, and an AdCom member of the IEEE Council on RFID serving as the Vice President of conferences. He is a Distinguished Lecturer of the IEEE Council on RFID. In 2016, his proposal for Inkjet/3-D printed millimeter-wave systems received the Bell Labs Prize, third place among more than 250 proposals recognizing ideas that change the game in the field of information and communications technologies.